Journal of Applied Engineering Mathematics

Volume 12, December 2025

Modeling Effective Laser Kerf in a Thin Wooden Plate

Benjamin Diehl

Mechanical Engineering Department
Brigham Young University
Provo, Utah 84602
bpdiehl@byu.edu

Abstract

Laser-cut wooden puzzles rely on tightly controlled kerf width to achieve good fit, strength, and aesthetics. This work models a thin basswood plate heated by a moving Gaussian surface flux representing a CO_2 laser. The 3D transient temperature field is obtained using finite Fourier transforms in x, y, and z, a Laplace transform in time, and numerical time convolution implemented in MATLAB. An effective kerf is defined as the surface region where $T(x, y, 0, t)$ exceeds an ablation threshold. The model reproduces expected trends with scan speed and provides a first-order tool for selecting cutting parameters and guiding more detailed future ablation models.

Nomenclature

L, M, H	Plate length, width, and thickness (m).
ρ	Density of wood (kg/m^3).
c	Specific heat (J/(kg K)).
k	Thermal conductivity (W/(m K)).
$\alpha = k/(\rho c)$	Thermal diffusivity (m^2/s).
$T(x, y, z, t)$	Temperature field (K).
$u(x, y, z, t)$	Temperature rise above ambient, $u = T - T_0$ (K).
T_0	Initial/ambient temperature (K).
T_{abl}	Ablation/char temperature threshold (K).
x_0, y_0	Initial laser beam center on the surface $z = 0$ (m).
v	Laser scan speed in the $+x$–direction (m/s).
ω_0	$1/e^2$ radius of the laser spot (m).
P	Laser power (W).
F_0	Peak incident heat flux, $F_0 = 2P/(\pi\omega_0^2)$ (W/m^2).
α_ℓ	Effective surface absorptivity (–).
$q''(x, y, t)$	Applied laser heat flux at $z = 0$ (W/m^2).

Introduction

3D wooden puzzles are often made by cutting and engraving a thin basswood with a CO_2 laser. By varying power and speed as the laser moves across the surface, a designer can engrave or cut designs as the laser ablates material. When a cut is made, the width of the cut is called the kerf, and is highly dependent on power and travel speed. Kerf width affects the fit, strength, and aesthetics when pieces are joined together.

Accurately modeling the laser cutting and etching process is difficult. A complex three-dimensional transient model for laser machining of ablating/decomposing materials has previously been developed by Modest, wherein he models the moving laser as a surface flux boundary condition, and demonstrates the ability to accurately define kerf, groove shape, temperature distribution, heat affected zones, etc. and accounts for variable properties[1].

Here we present a simplified approach using the Finite Fourier Transform method and a Laplace transform, providing simplified first-order accuracy for kerf as a function of laser power and travel speed[2].

Governing Equations and Assumptions

We start with the 3D cartesian heat transfer equation for an isotropic rectangular solid with $u(x,y,z,t) = T(x,y,z,t) - T_0$

$$\begin{aligned} &\frac{1}{\alpha}\frac{\partial u}{\partial t} = \frac{\partial^2 u}{\partial x^2} + \frac{\partial^2 u}{\partial y^2} + \frac{\partial^2 u}{\partial z^2}, \\ &0 < x < L,\ 0 < y < M,\ 0 < z < H,\ t > 0, \end{aligned} \tag{1}$$

with initial condition

$$u(x,y,z,0) = 0. \tag{2}$$

We transfer the x and y boundary conditions used by Modest to finite space [1],

$$u(0,y,z,t) = 0, \qquad u(L,y,z,t) = 0, \tag{3}$$

$$u(x,0,z,t) = 0, \qquad u(x,M,z,t) = 0, \tag{4}$$

but modify the z boundary conditions. As we will not account for ablation, we apply the moving laser as a forced heat flux only on the top surface, moving in x-y space and time,

$$-k\ \left.\frac{\partial u}{\partial z}\right|_{z=0} = q''(x,y,t). \tag{5}$$

Whereas most laser cutters have a supporting honeycomb structure that restricts cooling air movement, we assume that the bottom surface of the material is insulated,

$$\left.\frac{\partial u}{\partial z}\right|_{z=H} = 0. \tag{6}$$

We model the laser heat flux as a gaussian spot that moves in the $+x$–direction with constant speed v,

$$q''(x,y,t) = \alpha_\ell F_0 \exp\left[-\frac{2\left[(x - x_0 - vt)^2 + (y - y_0)^2\right]}{\omega_0^2}\right] \tag{7}$$

To simplify, we treat the surface as a perfect absorber ($\alpha_\ell = 1$), and ignore all other radiation effects, moisture effects, phase changes, laser focus, laser pulsing, etc.

Solution Method

To solve this PDE, we apply the Finite Fourier Transform method in x, y, and z, denoting eigenvalues and eigenfunctions as μ_n, ν_m, ζ_ℓ, and $X_n(x)$, $Y_m(y)$, and $Z_\ell(z)$ respectively. We introduce a separation eigenvalue $\lambda_{nm\ell}$ where

$$\lambda_{nm\ell} = \mu_n^2 + \nu_m^2 + \zeta_\ell^2. \tag{8}$$

All boundary conditions were also transformed. The top surface boundary condition moves into the thrice transformed equation as $\bar{q}_{nm}(t)$

$$\frac{1}{\alpha}\frac{\partial}{\partial t}\bar{u}_{nm\ell} = -\lambda_{nm\ell}\bar{u}_{nm\ell}(t) - \bar{q}_{nm}(t). \tag{9}$$

A Laplace transform is then taken, and with the transformed initial condition, we get the Laplace-domain equation

$$\frac{s}{\alpha}U(s) = -\lambda_{nm\ell}U(s) - Q(s), \tag{10}$$

where $Q(s) = \mathcal{L}\{\bar{q}_{nm}(t)\}$. Solving for $U(s)$ results in

$$U(s) = \frac{-\alpha Q(s)}{\frac{s}{\alpha} + \lambda_{nm\ell}}. \tag{11}$$

The inverse-Laplace transform results in the convolution

$$\bar{u}_{nm\ell}(t) = -\alpha \int_0^t e^{-\alpha\lambda_{nm\ell}(t-\tau)}\bar{q}_{nm}(t)\,d\tau, \tag{12}$$

where

$$\bar{q}_{nm}(t) = \int_0^M \int_0^L q''(x,y,t)X_n(x)Y_m(y)\,dx\,dy, \tag{13}$$

and the inverse Fourier transform in x, y and z results in

$$u(x,y,z,t) = \sum_{n=1}^{\infty}\sum_{m=1}^{\infty}\sum_{\ell=0}^{\infty}\bar{u}_{nm\ell}(t)\,X_n(x)\,Y_m(y)\,Z_\ell(z) \tag{14}$$

which can then be used to re-construct the temperature field with $T(x,y,0,t) = T_0 + u(x,y,0,t)$.

Numerical Implementation

By plotting the solution derived in eq.38 for various laser tracing speeds v we can determine how kerf depends on

laser movement speed. For our model, we used a small size of basswood $L = M = 4in, H = 1/8in$ with thermal constants $k = 0.05W/(m°\mathrm{C}), \rho = 415kg/m^3, c = 340J/(kg°\mathrm{C}), T_0 = 298.15$. Basswood has a minimum ablation temperature $T_{abl} = 473.15$. The power and gasssian spreading of the laser were typical of $P = 60W, \omega = 200\mu m$.

The velocity of the moving laser was set to 10, 30, 50, and 70mm/s, which is a typical range of values for a laser cutter.

The kerf was estimated as the y-dimensional width where $T > T_{abl}$ at z = 0. Since multiple passes are often needed to cut completely through basswood with a 60W laser, and the material has time to cool between each pass, this is a reasonable, first-order approximation.

Kerf tends to be very small (no more than 0.04"), so a large grid resolution in y was needed, giving a y-dimensional size of 0.005".

Odd-number of terms and odd numbers of resolution in each dimension (especially in y) were used, as due to symmetry the laser flux was chosen to be applied at $y = M/2$ starting at $x = L/4$. Using an even number of terms or an even resolution causes the location where the temperature is evaluated to straddle the peak of the gaussian laser source, dramatically decreasing the apparent flux.

Results

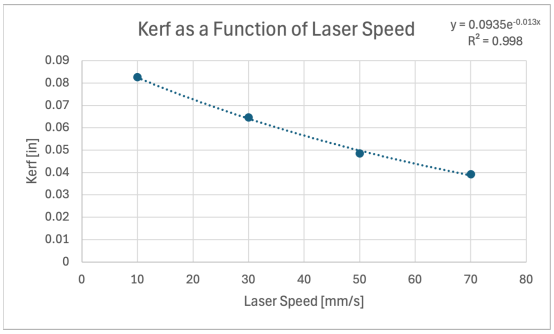

Figure 1: Kerf as a function of laser speed for a 60W CO_2 laser cutting 1/8" basswood.

Figure 1 shows the predicted effective kerf width as a function of laser scan speed for a 60 W CO_2 laser cutting 1/8" basswood. For the parameters listed in the Numerical Implementation section, the model predicts small kerf values, on the order of a fraction of a millimeter (less than 0.04"). As expected, slower scan speeds yield larger kerf widths because more energy is deposited per unit length of cut, while faster scan speeds reduce the time-averaged heating at a given location and therefore produce narrower kerf.

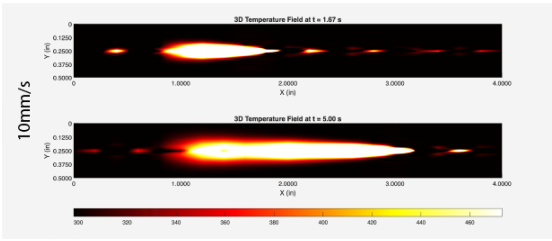

Figure 2: Temperature distribution on laser surface for 10mm/s

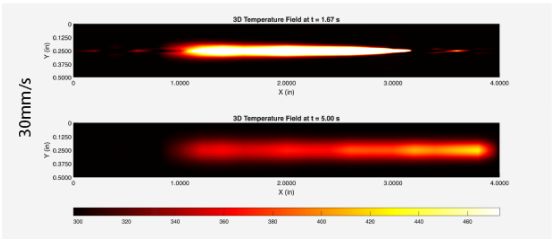

Figure 3: Temperature distribution on laser surface for 30mm/s

Surface temperature fields at $z = 0$ for representative scan speeds are shown in Figures 2–5. In all cases, the hottest region is localized near the beam center and elongated in the direction of motion, with a modest thermal wake trailing the laser. The temperature distribution is symmetric about the midline in y by construction, and remains well confined relative to the plate dimensions L and M, justifying the use of finite-sine eigenfunctions in x and y.

The 3D model also indicates that, for the chosen parameter set, the heat penetration in the thickness direction is limited over the time scale of a single pass. Peak temperatures are attained near the top surface, while the insulated back surface at $z = H$ remains significantly cooler. This

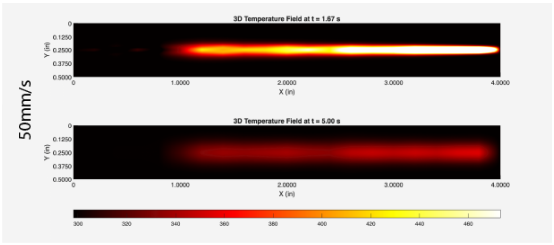

Figure 4: Temperature distribution on laser surface for 50mm/s

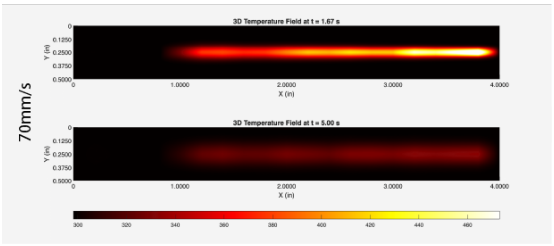

Figure 5: Temperature distribution on laser surface for 70mm/s

behavior is consistent with the practical observation that multiple passes can be required to fully cut through 1/8" basswood with a 60 W laser, even when the surface region locally exceeds the ablation temperature.

Discussion

Overall, the results match what most users intuitively see when working with a CO_2 laser: slower speeds dump more energy into the wood, the surface heats up more, and the kerf widens; faster speeds give the beam less time to heat any single point, so the temperature barely reaches the ablation threshold and the kerf becomes very narrow. The model captures this behavior directly through the $1/v$ dependence in the moving Gaussian flux.

The solution also helps show how material and laser parameters influence the cut. The thermal diffusivity $\alpha = k/(\rho c)$ controls how quickly heat spreads out from the beam. Woods with higher conductivity or lower heat capacity distribute heat faster, which broadens the warm region but reduces the peak temperature. The Gaussian spot size ω_0 works the same way: a smaller beam radius concentrates the flux and releases a higher temperature rise, while a larger beam naturally produces a thicker heat band even before considering motion.

There are still important limitations worth noting. The model does not include any explicit ablation or material removal—it only identifies where the temperature exceeds a chosen threshold. Wood properties are taken as constant, even though they vary significantly with temperature and moisture content. And the boundary conditions are intentionally simplified: real laser cutters involve radiative losses, airflow through the honeycomb, and additional convection from exhaust systems. These effects would change the exact temperature field but not the overall trends.

Even with the simplifications, this 3D transient formulation provides a helpful middle-ground between very simple 1D/2D approximations and full ablation models like Modest's. It gives a fast way to estimate how power, speed, and spot size affect kerf, and it makes it much easier to explore parameter changes inside MATLAB before doing physical tests.

Conclusions

This paper presented a 3D transient heat-transfer model for a thin wooden plate heated by a moving Gaussian laser flux. By applying finite Fourier transforms in all three spatial dimensions and a Laplace transform in time, we obtained a solution that can be evaluated efficiently in MATLAB using eigenfunction expansions and time convolution.

For a 60 W CO_2 laser cutting 1/8" basswood, the model predicts kerf width on the order of 0.04", with a clear and consistent trend: kerf decreases as scan speed increases. The temperature field remains localized near the surface, and penetration through the full thickness during a single pass is limited. This aligns well with practical experience that multiple passes are typically required to cut through basswood cleanly.

The strength of this model is that it provides a fast, first-order way to connect laser settings (power, speed, spot size) to thermal behavior and resulting kerf. It offers a practical tool for choosing cutting parameters before experimenting on real material. Future work should incorporate temperature-dependent properties, include more real-

istic thermal losses, and eventually couple the model to a true ablation or char front so that kerf is predicted from material removal rather than a temperature threshold.

Acknowledgements

Dr. Vladimir Soloviev for the reference to Modest's paper, and resources in the *Integrated Engineering Mathematics* textbook.

ChatGPT for helping find MATLAB code errors and make plotting easier

References

[1] Michael F. Modest. "Three-dimensional, transient model for laser machining of ablating/decomposing materials". In: *International Journal of Heat and Mass Transfer* 39.2 (1996), pp. 221–234. ISSN: 0017-9310. DOI: https://doi.org/10.1016/0017-9310(95)00134-U. URL: https://www.sciencedirect.com/science/article/pii/001793109500134U.

[2] Vladimir Solovjov. "Finite Fourier Transform". In: *Integrated Engineering Mathematics*. Provo, Utah: Brigham Young University, 2025. Chap. IX.3, pp. 755–766.

Appendix

Appendix A: Finite Fourier Transform Derivation

In this appendix we outline the full derivation of the transient temperature rise $u(x, y, z, t) = T(x, y, z, t) - T_0$ in the thin plate, using a finite Fourier transform in the three spatial coordinates.

A.1 Governing equation and boundary conditions

We model the temperature rise with the 3D heat equation

$$\frac{1}{\alpha}\frac{\partial u}{\partial t} = \frac{\partial^2 u}{\partial x^2} + \frac{\partial^2 u}{\partial y^2} + \frac{\partial^2 u}{\partial z^2}, \quad 0 < x < L,\ 0 < y < M,\ 0 < z < H,\ t > 0, \tag{15}$$

with initial condition

$$u(x, y, z, 0) = 0. \tag{16}$$

The lateral boundaries are taken to be held at ambient temperature,

$$u(0, y, z, t) = 0, \qquad u(L, y, z, t) = 0, \tag{17}$$

$$u(x, 0, z, t) = 0, \qquad u(x, M, z, t) = 0, \tag{18}$$

while the lower surface $z = H$ is assumed insulated,

$$\left.\frac{\partial u}{\partial z}\right|_{z=H} = 0, \tag{19}$$

and the upper surface $z = 0$ is heated by the moving laser,

$$-k\left.\frac{\partial u}{\partial z}\right|_{z=0} = q''(x, y, t). \tag{20}$$

The laser heat flux is modeled as a Gaussian spot that translates in the $+x$–direction with constant speed v,

$$q''(x, y, t) = \alpha_\ell F_0 \exp\left[-\frac{2\left[(x - x_0 - vt)^2 + (y - y_0)^2\right]}{\omega_0^2}\right] \tag{21}$$

A.2 Finite Fourier Transform in x, y, and z

In the x–direction with Dirichlet–Dirichlet conditions (17) we obtain

$$X_n(x) = \sin(\mu_n x), \qquad \mu_n = \frac{n\pi}{L}, \quad n = 1, 2, \ldots \tag{22}$$

with norm

$$\|X_n\|^2 = \int_0^L X_n^2(x)\, dx = \frac{L}{2}, \tag{23}$$

and operational property

$$\int_0^L \left(\frac{\partial^2 u}{\partial x^2}\right) X_n(x)\, dx = -\mu_n^2 \bar{u_n} + f_0 X_n'(0) - f_L X_n'(L) \tag{24}$$

where $f_0 = f_L = 0$.

In the y–direction with Dirichlet–Dirichlet conditions (18),

$$Y_m(y) = \sin(\nu_m y), \qquad \nu_m = \frac{m\pi}{M}, \quad m = 1, 2, \dots \tag{25}$$

with norm

$$\|Y_m\|^2 = \int_0^M Y_m^2(y)\, dy = \frac{M}{2}, \tag{26}$$

and operational property

$$\begin{aligned} &\int_0^M (\frac{\partial^2}{\partial y^2}\bar{u}_n(y,z,t))Y_m(y)\, dy = \\ &-\nu_m^2 \bar{u}_{nm} + f_0 Y_n'(0) - f_M Y_n'(M) \end{aligned} \tag{27}$$

where $f_0 = f_M = 0$.

In the z–direction we apply the non-homogeneous Neumann conditions at $z = 0$ and $z = H$ for the eigenvalue problem,

$$Z_\ell''(z) + \zeta_\ell^2 Z_\ell(z) = 0, \tag{28}$$

so that

$$\begin{aligned} &Z_0 = 1, \qquad \zeta_0 = 0 \\ &Z_\ell(z) = \cos(\zeta_\ell z), \qquad \zeta_\ell = \frac{\ell\pi}{H}, \quad \ell = 0, 1, 2, \dots \end{aligned} \tag{29}$$

with norms

$$\begin{aligned} \|Z_0\|^2 &= \int_0^H 1^2\, dz = H, \\ \|Z_\ell\|^2 &= \int_0^H \cos^2(\zeta_\ell z)\, dz = \frac{H}{2}, \quad \ell \geq 1 \end{aligned} \tag{30}$$

and operational property

$$\begin{aligned} &\int_0^H (\frac{\partial^2}{\partial z^2}\bar{u}_{nm}(z,t))Z_\ell(y)\, dz = \\ &-\zeta_\ell^2 \bar{u}_{nm\ell} - f_0 Z_\ell(0) + f_H Z_\ell(H) \end{aligned} \tag{31}$$

where $f_0 = \bar{q}_{nm}(t)$ and $f_H = 0$.

Note that $Z_\ell(0) = 1$ for all ℓ.

Combining FFTs in x, y and z results in

$$\begin{aligned} &\frac{1}{\alpha}\frac{\partial}{\partial t}\bar{u}_{nm\ell}(t) \\ &= -\mu_n^2 \bar{u}_{nm\ell}(t) - \nu_m^2 \bar{u}_{nm\ell}(t) - \zeta_\ell^2 \bar{u}_{nm\ell}(t) - \bar{q}_{nm}(t). \end{aligned} \tag{32}$$

We make the simplification of $\lambda_{nm\ell} = \mu_n^2 + \nu_m^2 + \zeta_\ell^2$

$$\frac{1}{\alpha}\frac{\partial}{\partial t}\bar{u}_{nm\ell} = -\lambda_{nm\ell}\bar{u}_{nm\ell}(t) - \bar{q}_{nm}(t), \tag{33}$$

where

$$\bar{q}_{nm}(t) = \int_0^M \int_0^L q''(x,y,t) X_n(x) Y_m(y)\, dx\, dy. \tag{34}$$

Equation (33) is now ready to be transformed to the laplace space.

A.3 Laplace Transform

A Laplace transform is then taken, and with the transformed initial condition, we get the Laplace-domain equation

$$\frac{s}{\alpha}U(s) = -\lambda_{nm\ell}U(s) - Q(s), \tag{35}$$

where $Q(s) = \mathcal{L}\{\bar{q}_{nm}(t)\}$. Solving for $U(s)$ results in

$$U(s) = \frac{-\alpha Q(s)}{\frac{s}{\alpha} + \lambda_{nm\ell}}. \tag{36}$$

A.4 Inverse Laplace and Inverse Fourier

The inverse-Laplace transform results in the convolution

$$\bar{u}_{nm\ell}(t) = -\alpha \int_0^t e^{-\alpha\lambda_{nm\ell}(t-\tau)} \bar{q}_{nm}(t)\, d\tau, \tag{37}$$

and the inverse Fourier transform in x, y and z results in

$$u(x,y,z,t) = \sum_{n=1}^{\infty}\sum_{m=1}^{\infty}\sum_{\ell=0}^{\infty} \bar{u}_{nm\ell}(t)\, X_n(x)\, Y_m(y)\, Z_\ell(z) \tag{38}$$

which can then be used to re-construct the temperature field with $T(x,y,0,t) = T_0 + u(x,y,0,t)$.

In practice, the sums over n, m, and ℓ are truncated at $n_{\max}$, $m_{\max}$, and $\ell_{\max}$.

